

PAPER

EXIT Chart-Aided Design of LDPC Codes for Self-Coherent Detection with Turbo Equalizer for Optical Fiber Short-Reach Transmissions

Noboru OSAWA^{†a)}, Student Member, Shinsuke IBI^{†b)}, Koji IGARASHI^{†c)}, Members, and Seiichi SAMPEI^{†d)}, Fellow

SUMMARY This paper proposed an iterative soft interference canceller (IC) referred to as turbo equalizer for the self-coherent detection, and extrinsic information transfer (EXIT) chart based irregular low density parity check (LDPC) code optimization for the turbo equalizer in optical fiber short-reach transmissions. The self-coherent detection system is capable of linear demodulation by a single photodiode receiver. However, the self-coherent detection suffers from the interference induced by signal-signal beat components, and the suppression of the interference is a vital goal of self-coherent detection. For improving the error-free signal detection performance of the self-coherent detection, we proposed an iterative soft IC with the aid of forward error correction (FEC) decoder. Furthermore, typical FEC code is no longer appropriate for the iterative detection of the turbo equalizer. Therefore, we designed an appropriate LDPC code by using EXIT chart aided code design. The validity of the proposed turbo equalizer with the appropriate LDPC is confirmed by computer simulations.

key words: self-coherent detection, turbo equalizer, LDPC, EXIT chart, optical fiber short-reach transmissions

1. Introduction

Detection of complex amplitudes in optical fiber transmissions, so-called linear demodulation, is capable of utilizing higher order modulation as well as digital domain dispersion compensation. Although the coherent reception, which is a typical method of linear demodulation, is applied to long-haul transmissions [1], the high-cost coherent receiver is not acceptable to cost-sensitive short-reach transmissions. Therefore, linear demodulation schemes with direct detection (DD) using a single photodiode (PD) have attracted much attention in recent years [2], [3]. One of the linear demodulation schemes based on DD is self-coherent detection which allocates a pilot tone around the edge of the baseband spectrum [4], [5]. In principle, the self-coherent detection captures pilot-signal beat components as the desired signals, while suppressing interference caused by signal-signal beat components. When the frequency gap between the pilot tone and the edge of baseband spectrum is wider than the width

of the data spectrum, it is free from interference problems. However, it results in requiring more than twice bandwidth of that for the data signal, and requires an expensive broader band PD.

Along with the evolution of digital signal processing (DSP) in optical communications, two types of signal detector have been developed for reducing the frequency gap: Kramers-Kronig (KK) detector [5] and iterative interference canceller (IC) [4]. The KK receiver individually detects the amplitude and phase of the signals. Since the amplitude is a square root of directly detected signal, the impairment caused by interference appears only in the phase detection. In phase detection of the KK receiver, square root and logarithm operations are applied to received signals. In this paper, we assume the system without optical amplifier and the thermal noise limit scenario for ease of analysis. Even in thermal noise limit scenario, the operations of the KK receiver complicate the stochastic behavior of noise, due to the presence of square root and logarithm operations. From the perspective of the transmission systems, the comprehensive design of forward error correction (FEC) and modulation play an important role in improving the signal detection capability. In the case of KK receiver, it is difficult to design the optimal code in its complicated stochastic signal model. For taking full advantage of the FEC, alternative DD scheme from KK, whose signal model is much more simple, is desirable.

On the other hand, iterative IC mitigates the interference by subtracting interference replicas from the received signals after generating the replica according to previously detected signals. Fortunately, the probabilistic model of IC is simpler than KK and suitable for analysis in linear algebraic representation. Therefore, this paper focuses on the iterative IC in terms of the comprehensive design of the transceiver. The capability of IC deeply relies on the accuracy of the replica generation. In [4], the interference replica is generated from hard decision symbols. Nevertheless, hard decision errors cause error propagation during the iterative IC process. For suppressing the harmful impacts of the error propagation, iterative soft IC with the assistance of FEC decoder is a rational canceller scheme. The iterative soft IC is referred to as turbo equalizer [6], [7]. The soft IC generates soft replica that is an expected value of the replica conditioned by FEC decoder outputs. The value of expectation reflects the reliability of FEC decoding.

Manuscript received September 19, 2018.

Manuscript revised November 29, 2018.

Manuscript publicized January 16, 2019.

[†]The authors are with the Graduate School of Engineering, Osaka University, Suita-shi, 565-0871 Japan.

a) E-mail: osawa@wcs.comm.eng.osaka-u.ac.jp

b) E-mail: ibi@comm.eng.osaka-u.ac.jp

c) E-mail: iga@comm.eng.osaka-u.ac.jp

d) E-mail: sampei@comm.eng.osaka-u.ac.jp

DOI: 10.1587/transcom.2018EBP3267

The first contribution of this paper is revealing how to design the soft IC according to the stochastic signal model for self-coherent systems. Furthermore, typical FEC code, which is optimized for additive white Gaussian noise (AWGN) channels, is no longer appropriate for the turbo equalizer. Subsequently, we design an appropriate irregular low density parity check (LDPC) code in terms of extrinsic information transfer (EXIT) analysis based on turbo principle [8]. The derived stochastic signal model plays a vital role for optimization of EXIT chart aided code design. This paper does not deal with impairments induced by optical noise. Of course, the mathematical stochastic model with the optical noise is very important and it would require more complicated algorithm for iterative soft IC depending on the probability distribution of the optical noise. This issue is remained as a future work.

The contributions of the present paper are summarized as follows:

- A structure of the iterative soft IC for the self-coherent detection is designed.
- A stochastic model of the self-coherent detection is revealed for generation of the soft interference replica.
- Irregular LDPC code is optimized for the self-coherent turbo receiver.

The present paper is organized as follows. In Sect. 2, we describe the system model of self-coherent linear demodulation under direct detection (DD) systems. In Sect. 3, turbo equalizer for the self-coherent detection is proposed. Moreover, the generation process of soft interference replica is mathematically revealed. In Sect. 4, irregular LDPC codes are optimized on the basis of EXIT analysis for the proposed turbo equalizer. In Sect. 5, results of computer simulations validate the iterative soft IC with the aid of the optimized LDPC codes. The conclusions are presented in Sect. 6.

Mathematical Notations: Throughout this paper, vectors and matrices are denoted by lower- and upper-case bold-face letters, respectively. Furthermore, \cdot^* , \cdot^T , and \cdot^H are the conjugate, transpose, and conjugate transpose (Hermite) operators, respectively. Unless otherwise specified, indexes of vectors and matrices start from 0 in this paper. Diagonal matrix with the elements of vector \mathbf{a} is denoted by $\text{diag}[\mathbf{a}]$. Trace of matrix \mathbf{A} is denoted by $\text{tr}[\mathbf{A}]$. $\mathbf{A} \circ \mathbf{B}$ indicates an element-wise (Hadamard) product of matrices. \mathbf{I}_a , $\mathbf{O}_{a \times b}$ and $\mathbf{1}_{a \times b}$ are identity matrix with size of $a \times a$, zero matrix with size of $a \times b$ and matrix of ones with size of $a \times b$. \mathbf{F}_X represents X points discrete Fourier transform (DFT) matrix which is defined as

$$\mathbf{F}_X = \frac{1}{\sqrt{X}} [\mathbf{f}_{X,0}, \dots, \mathbf{f}_{X,x}, \dots, \mathbf{f}_{X,X-1}], \quad (1)$$

$$\mathbf{f}_{X,x} = \left[e^{-j2\pi \frac{0x}{X}}, e^{-j2\pi \frac{1x}{X}}, \dots, e^{-j2\pi \frac{(X-1)x}{X}} \right]^T. \quad (2)$$

When \mathbf{a} denotes time domain components, $\underline{\mathbf{a}}$ implies frequency domain representations of \mathbf{a} . $Pr[a|b]$ and $p(a|b)$ are probability mass and density functions of a conditioned by b , respectively. $\mathbb{E}\{\mathbf{a}\}$ represents the expectation value of \mathbf{a} .

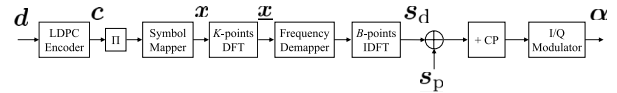


Fig. 1 Schematic of transmitter for self-coherent detection.

On the other hand, $\mathbb{E}_b\{\mathbf{a}\}$ means the expectation value of \mathbf{a} conditioned by b .

2. Self-Coherent Detection

2.1 Configuration of Transmitter

A schematic of the transmitter is illustrated in Fig. 1. For the ease of analysis, we assume that the transmit signal obeys DFT-spread OFDM signaling, which is a kind of broadband single carrier block transmissions, with low peak to average power ratio (PAPR) [9]. However, in practice, the signaling can be replaced by the appropriate analog filter for minimizing the bandwidth of signals in DSP. Let M , N , and K be information, code, and symbol lengths in one block. At the transmitter, information bits $\mathbf{d} \in \{0, 1\}^{M \times 1}$ are encoded by an LDPC encoder. The resultant coded bits are denoted by $\mathbf{c} \in \{0, 1\}^{N \times 1}$. The vector \mathbf{c} is interleaved and mapped to complex data symbols. A vector of the derived data symbols is represented by $\mathbf{x} = [x[0], x[1], \dots, x[k], \dots, x[K-1]]^T \in \mathbb{C}^{K \times 1}$. The average energy of data symbols is denoted by $E_s = \mathbb{E}\{\mathbf{x}^H \mathbf{x}\} / K$. In the DFT-spread OFDM, the spectrum of data symbols is shaped in the frequency domain. By applying K -points DFT to \mathbf{x} as

$$\underline{\mathbf{x}} = \mathbf{F}_K \mathbf{x}, \quad (3)$$

the shaped signals in time and frequency domain representations are respectively derived by

$$\mathbf{s}_d = \mathbf{F}_B^H \underline{\mathbf{s}}_d, \quad (4)$$

$$\underline{\mathbf{s}}_d = \mathbf{M}_\theta \underline{\mathbf{x}}^T, \quad (5)$$

where $\mathbf{M}_\theta = [\mathbf{O}_{K \times \theta}, \mathbf{I}_K, \mathbf{O}_{K \times (B-K-\theta)}]$ is a spectrum shaping matrix, and θ is the frequency offset and $B (> 2K)$ is the number of whole frequency bins for the digital signal processing. As a result, the shaping matrix assigns the contiguous data spectrum $\underline{\mathbf{x}}$ between the θ -th and $(\theta + K - 1)$ -th bins. Note that analog bandpass filter is applicable instead of the spectrum shaping of DFT-spread OFDM. For the ease of analysis, DFT-based shaping is applied in this paper.

To assign a pilot tone at the ϕ -th frequency bin, the pilot signal \mathbf{s}_p in the time domain is superpositioned to \mathbf{s}_d , which is expressed as

$$\mathbf{s} = \mathbf{s}_d + \mathbf{s}_p. \quad (6)$$

The pilot tone signal is given by

$$\mathbf{s}_p = \sqrt{\frac{E_p}{B}} \mathbf{f}_{B,\phi}^*. \quad (7)$$

The energy of the pilot signal is $\mathbb{E}\{\mathbf{s}_p^H \mathbf{s}_p\} = E_p$, resulting in

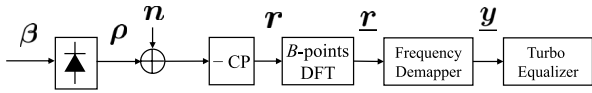


Fig. 2 Schematic of receiver for self-coherent detection with turbo equalizer.

$\mathbb{E}\{s^H s\} = \mathbb{E}\{s_d^H s_d\} + \mathbb{E}\{s_p^H s_p\} = \mathbb{E}\{x_d^H x_d\} + E_p = K E_s + E_p$. Since direct-current (DC) components are inconvenient for low-cost devices, the frequency offset ϕ should be little away from DC.

To permit of one-tap frequency domain equalization (FDE) at the receiver, cyclic prefix (CP) is appended in front of s . If in the case that usage of CP is not acceptable, overlap FDE technique [10] is available instead. Without loss of generality, the signals with and without CP are denoted by the same variable, for ease of the mathematical notations. After the electrical signal processing, the resultant signal with CP is converted to an optical signal by optical I/Q modulator. Supposing that the optical I/Q modulation is ideally linear, the optical signal is expressed as

$$\alpha = \Psi s, \quad (8)$$

where Ψ is a diagonal weight matrix of the linear modulation. Optical signal α is delivered to the receiver via an optical fiber.

2.2 Configuration of Receiver

A schematic of the receiver with turbo equalizer is illustrated in Fig. 2. This paper assumes the system without optical amplifier and the thermal noise limit scenario. Therefore, the optical noise such as shot noise is negligibly small compared with the circuit noise. The received optical signal in discrete time domain representation is expressed as

$$\beta = \Omega \alpha = \Xi s, \quad (9)$$

where $\Xi = \Omega \Psi$ and Ω is a Toeplitz channel matrix with channel memory, which is determined by fiber characteristics such as chromatic dispersion [11]. The received signal is directly detected by a photo diode. Assuming that the photo diode is an ideal square-law detector, electrical amplitude of the directly detected signal is represented by

$$\rho = \beta \circ \beta^* = \rho_{dd} + \rho_{pp} + \rho_{dp} + \rho_{dp}^*. \quad (10)$$

The resultant ρ consists of signal-signal beat $\rho_{dd} = (\Xi s_d) \circ (\Xi s_d)^*$, pilot-pilot beat $\rho_{pp} = (\Xi s_p) \circ (\Xi s_p)^*$, and signal-pilot beat $\rho_{dp} = (\Xi s_d) \circ (\Xi s_p)^*$.

After sampling the ideal square-law detector outputs with an appropriate time interval, CP parts are removed from the observations. In this case, the channel matrix Ξ in Eq. (9) can be regarded as a $B \times B$ circulant matrix whose first column vector ξ corresponds to channel impulse response (CIR). On the basis of DFT matrix F_B , the circulant matrix Ξ can be diagonalized as

$$\Xi = F_B \Xi F_B^H, \quad (11)$$

where

$$\Xi = \text{diag}[\xi], \quad (12)$$

$$\xi = \sqrt{B} F_B \xi \in \mathbb{C}^{B \times 1}. \quad (13)$$

The diagonalization is helpful in FDE process for shrinking the computational complexity.

Under the assumptions mentioned above, the beat components are expressed as

$$\rho_{dd} = [\rho_{dd}[0], \dots, \rho_{dd}[B-1]]^T, \quad (14)$$

$$\rho_{dd}[b] = \frac{1}{B} \sum_{i=0}^{B-1} \sum_{j=0}^{B-1} e^{j2\pi \frac{(i-j)b}{B}} \xi[i] s_d[i] \xi^*[j] s_d^*[j], \quad (15)$$

$$\rho_{pp} = \frac{E_p}{B} |\xi[\phi]|^2 \mathbf{1}_{B \times 1}, \quad (16)$$

$$\rho_{dp} = \sqrt{\frac{E_p}{B}} \xi^*[\phi] \Theta_\phi \Xi s_d, \quad (17)$$

where $\Theta_\phi = \text{diag}[f_{B,\phi}]$. The detailed derivations of ρ_{dd} , ρ_{pp} , and ρ_{dp} are described in Appendix A.

Assuming a thermal noise limit scenario, the detected signal suffering from electrical noise is expressed as

$$r = \rho + n, \quad (18)$$

where $n \in \mathbb{R}^{B \times 1}$ denotes Gaussian noise vector whose elements have zero mean and variance of N_0 . After observing the received signal $r \in \mathbb{R}^{B \times 1}$, B points DFT is applied as

$$\underline{r} = F_B r = F_B [\rho_{dd} + \rho_{pp} + \rho_{dp} + \rho_{dp}^* + n]. \quad (19)$$

Let us focus on the signal-pilot beat component in the frequency domain representation, which is expressed as

$$\underline{\rho}_{dp} = F_B \rho_{dp} = \sqrt{\frac{E_p}{B}} \xi^*[\phi] \Theta_\phi \Xi s_d, \quad (20)$$

where we have

$$\Theta_\phi = F_B \Theta_\phi F_B^H = \begin{bmatrix} \mathbf{O}_{(B-\phi) \times \phi} & \mathbf{I}_{B-\phi} \\ \mathbf{I}_\phi & \mathbf{O}_{\phi \times (B-\phi)} \end{bmatrix}. \quad (21)$$

Because Ξ is a diagonal matrix, Θ_ϕ can be applied as $\Theta_\phi \Xi s_d = \text{diag}[\Theta_\phi \xi] \Theta_\phi s_d$. Substituting Eq. (5) into Eq. (20), $\underline{\rho}_{dp}$ is rewritten as

$$\begin{aligned} \underline{\rho}_{dp} &= \sqrt{\frac{E_p}{B}} \xi^*[\phi] \Theta_\phi \Xi M_\theta \underline{x} \\ &= \sqrt{\frac{E_p}{B}} \xi^*[\phi] \text{diag}[\Theta_\phi \xi] \\ &\quad \cdot [\mathbf{O}_{1 \times \delta}, \underline{x}^T, \mathbf{O}_{1 \times (B-\delta-K)}]^T, \end{aligned} \quad (22)$$

where $\delta = \theta - \phi$ indicates the gap between the pilot tone and the edge of data spectrum. Therefore, to extract \underline{x} from \underline{r} , the spectrum is demapped as

$$\underline{y} = [r[\delta], \dots, r[\delta + K - 1]]^T = M_\delta^T \underline{r}. \quad (23)$$

where $M_\delta = [\mathbf{O}_{K \times \delta}, \mathbf{I}_K, \mathbf{O}_{K \times (B-K-\delta)}]$. Taking into account the fact that the components of $\mathbf{F}_B \rho_{pp}$ and $\mathbf{F}_B \rho_{dp}^*$ do not exist between $r[\delta]$ and $r[\delta + K - 1]$, $\underline{\mathbf{y}}$ can be expressed as

$$\begin{aligned} \underline{\mathbf{y}} &= \mathbf{M}_\delta^T \mathbf{F}_B (\rho_{dp} + \rho_{dd} + \mathbf{n}) \\ &= \underline{\mathbf{H}} \underline{\mathbf{x}} + \underline{\mathbf{v}} + \underline{\mathbf{z}}, \end{aligned} \quad (24)$$

where we have

$$\underline{\mathbf{H}} = \text{diag}[\underline{\mathbf{h}}], \quad (25)$$

$$\underline{\mathbf{h}} = \sqrt{\frac{E_p}{B}} \underline{\xi}^* [\phi] \mathbf{M}_\delta^T \underline{\Theta}_\phi \underline{\xi} = \sqrt{\frac{E_p}{B}} \underline{\xi}^* [\phi] \mathbf{M}_\delta^T \underline{\xi}, \quad (26)$$

$$\underline{\mathbf{v}} = \mathbf{M}_\delta^T \mathbf{F}_B \rho_{dd} = \mathbf{M}_\delta^T \underline{\rho}_{dd}, \quad (27)$$

$$\underline{\mathbf{z}} = \mathbf{M}_\delta^T \mathbf{F}_B \mathbf{n}. \quad (28)$$

Note that the elements of $\underline{\mathbf{z}}$ obey complex Gaussian distribution $\mathcal{CN}(0, N_0)$.

A main problem to be explored in this paper is how to detect the desired signal $\underline{\mathbf{x}}$ while shrinking the negative impacts of interference of $\underline{\mathbf{v}}$ in Eq. (24).

3. Turbo Equalizer

3.1 Iterative Demodulation and Decoding

Figure 3 illustrates a schematic of the turbo equalizer for self-coherent linear demodulation, which is used to mitigate interference of $\underline{\mathbf{v}} \in \mathbb{C}^{K \times 1}$. The turbo equalizer is capable of not only cancellation of signal-signal beat interference but also mitigating inter-symbol interference (ISI) induced by severe frequency selectivity of $\underline{\mathbf{H}}$ [12]. This paper assumes that the ISI caused by chromatic dispersion is small, but even if the channel is suffering from severe ISI, the technique of [12] is available. The turbo receiver is comprised of two modules: a soft-canceling minimum mean square error (MMSE) equalizer and channel (LDPC) decoder. The extrinsic LLRs are exchanged between the two modules for iteratively shrinking the interference on the basis of turbo principle [6], [7]. In the soft-canceling MMSE, soft interference replicas are subtracted from $\underline{\mathbf{y}}$. At the first iteration, no feedback is yielded from the LDPC decoder. However, at the second and later iteration, the decoder is capable of providing prior LLR to the equalizer. According to the obtained LLR, the replica generator outputs a vector of soft interference replicas $\hat{\underline{\mathbf{v}}} \in \mathbb{C}^{K \times 1}$. The detailed derivation of the replica vector is discussed in Sect. 3.2.1.

Firstly, the soft interference cancellation is conducted as

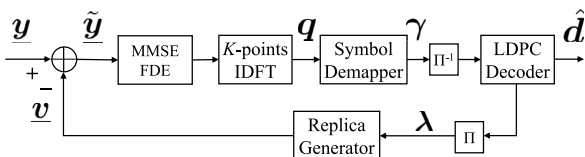


Fig. 3 Schematic of turbo equalizer.

$$\tilde{\underline{\mathbf{y}}} = \underline{\mathbf{y}} - \hat{\underline{\mathbf{v}}} = \underline{\mathbf{H}} \underline{\mathbf{x}} + \underline{\mathbf{z}} + (\underline{\mathbf{v}} - \hat{\underline{\mathbf{v}}}). \quad (29)$$

Then, FDE based on the MMSE criterion is applied for compensating the negative impacts of $\underline{\mathbf{v}}$ as well as the channel matrix $\underline{\mathbf{H}}$, which is experienced in optical fibers. The MMSE filter weight matrix \mathbf{W} is calculated by assuming that the residual interference $(\underline{\mathbf{v}} - \hat{\underline{\mathbf{v}}})$ obeys uncorrelated complex Gaussian distribution, whose covariance matrix is given by a diagonal matrix $\mathbb{E}_\lambda \{(\underline{\mathbf{v}} - \hat{\underline{\mathbf{v}}})(\underline{\mathbf{v}} - \hat{\underline{\mathbf{v}}})^H\} = \text{diag}[\underline{\mathbf{g}}]$ where we have the variance vector of $\underline{\mathbf{g}} = [g[0], \dots, g[K-1]]^T$. The FDE weight matrix \mathbf{W} is optimized to minimize the following mean-square error (MSE) [13]:

$$\text{MSE} = \mathbb{E}_\lambda \left\{ \left| \mathbf{W}^H \tilde{\underline{\mathbf{y}}} - \underline{\mathbf{x}} \right|^2 \right\}. \quad (30)$$

The resultant weight matrix is given by solving Wiener-Hopf equation as

$$\mathbf{W}^H = \left[\underline{\mathbf{H}} \underline{\mathbf{H}}^H + \frac{1}{E_s} (N_0 \mathbf{I}_K + \text{diag}[\underline{\mathbf{g}}]) \right]^{-1} \underline{\mathbf{H}}^H. \quad (31)$$

The derivation of variance vector $\underline{\mathbf{g}}$ is discussed in Sect. 3.2.2. After the FDE process $\mathbf{W}^H \tilde{\underline{\mathbf{y}}}$, K -points IDFT is applied to return to the time domain representation as

$$\begin{aligned} \mathbf{q} &= [q[0], \dots, q[K-1]]^T = \mathbf{F}_K^H \mathbf{W}^H \tilde{\underline{\mathbf{y}}} \\ &= \mathbf{F}_K^H \mathbf{W}^H \underline{\mathbf{H}} \mathbf{F}_K \mathbf{x} + \mathbf{F}_K^H \mathbf{W}^H (\underline{\mathbf{z}} + \underline{\mathbf{v}} - \hat{\underline{\mathbf{v}}}). \end{aligned} \quad (32)$$

Observing the FDE output \mathbf{q} , symbol demapper computes extrinsic LLR. For computing extrinsic LLR, scalar Gaussian approximation (SGA) is applied to each element of \mathbf{q} as

$$q[k] = \mu x[k] + v[k], \quad (33)$$

where the gain factor μ is approximately derived by

$$\mu = \mathbf{F}_K^H \mathbf{W}^H \underline{\mathbf{H}} \mathbf{F}_K \approx \frac{1}{K} \text{tr} [\mathbf{W}^H \underline{\mathbf{H}}], \quad (34)$$

and Gaussian noise term is

$$\nu = [\nu[0], \dots, \nu[K-1]]^T = \mathbf{F}_K^H \mathbf{W}^H (\underline{\mathbf{z}} + \underline{\mathbf{v}} - \hat{\underline{\mathbf{v}}}). \quad (35)$$

The covariance matrix of ν is approximately given by

$$\begin{aligned} \mathbb{E}_\lambda \{ \nu \nu^H \} &= \mathbf{F}_K^H \mathbf{W}^H \mathbb{E}_\lambda \{ (\underline{\mathbf{z}} + \underline{\mathbf{v}} - \hat{\underline{\mathbf{v}}}) (\underline{\mathbf{z}} + \underline{\mathbf{v}} - \hat{\underline{\mathbf{v}}})^H \} \mathbf{W} \mathbf{F}_K \\ &\approx \left(N_0 + \frac{1}{K} \sum_{k=0}^{K-1} g[k] \right) \mathbf{F}_K^H \mathbf{W}^H \mathbf{W} \mathbf{F}_K \\ &\approx \sigma_v^2 \mathbf{I}_K, \end{aligned} \quad (36)$$

where

$$\sigma_v^2 = \left(N_0 + \frac{1}{K} \sum_{k=0}^{K-1} g[k] \right) \frac{1}{K} \text{tr} [\mathbf{W} \mathbf{W}^H]. \quad (37)$$

According to the values of μ and σ_v^2 for describing Gaussian distribution, the extrinsic LLR related to a coded bit $c[l]$ is computed as

$$\gamma[l] = \frac{\sum_{X^+ \in \{\mathcal{X}|c[l]=1\}} \exp\left[-\frac{|q[k]-\mu X^+|^2}{\sigma_v^2}\right]}{\sum_{X^- \in \{\mathcal{X}|c[l]=0\}} \exp\left[-\frac{|q[k]-\mu X^-|^2}{\sigma_v^2}\right]}, \quad (38)$$

where $\{\mathcal{X}|c[l] = 0 \text{ or } 1\}$ means the subset of constellations belonging to $c[l] = 0$ or 1 . The extrinsic LLR sequence $\gamma = [\gamma[0], \dots, \gamma[L-1]]^T \in \mathbb{R}^{L \times 1}$ is deinterleaved, and provided to the LDPC decoder. In the channel decoder, extrinsic LLRs are computed by sum product algorithm (SPA). The derived LLRs are interleaved to form $\lambda = [\lambda[0], \dots, \lambda[L-1]]^T \in \mathbb{R}^{L \times 1}$, and yielded to the replica generator. At the final iteration step of the iterative detection after iteratively exchanging LLRs γ and λ , the information bits $\hat{\mathbf{d}}$ are detected at the channel decoder.

3.2 Generation of Soft Interference Replica

3.2.1 Soft Interference Replica Of $\underline{v}[k]$

The soft interference replica is theoretically defined by a conditional expectation of the interference random sources. In the turbo equalizer, extrinsic LLR λ is used as prior information. The expectation conditioned by λ is defined by

$$\hat{v}[k] = \mathbb{E}_\lambda \{v[k]\} = \mathbb{E}_\lambda \{\rho_{\text{dd}}[k']\}, \quad (39)$$

where $k' = k + \delta \in \{\delta, \dots, \delta + (K-1)\}$. Now, let us move our focus on the frequency component $\rho_{\text{dd}}[b]$ in ρ_{dd} . Taking into account the fact that Eq. (15) implies that all terms of $\rho_{\text{dd}}[b]$ are on the orthogonal Fourier basis, the frequency domain representation $\underline{\rho}_{\text{dd}} = \mathbf{F}_B \rho_{\text{dd}}$ can be simply derived from Eq. (15). More specifically, the b -th element of $\underline{\rho}_{\text{dd}}$ consists of the terms of $(i-j) = b$ or $(i-j) = b-B$, which is expressed as

$$\begin{aligned} \rho_{\text{dd}}[b] &= \frac{1}{\sqrt{B}} \sum_{i=0}^{(B-1)-b} \underline{\xi}[i+b] \underline{s}_{\text{d}}[i+b] \underline{\xi}^*[i] \underline{s}_{\text{d}}^*[i] \\ &+ \frac{1}{\sqrt{B}} \sum_{i=0}^{b-1} \underline{\xi}[i] \underline{s}_{\text{d}}[i] \underline{\xi}^*[i+B-b] \underline{s}_{\text{d}}^*[i+B-b]. \end{aligned} \quad (40)$$

In the turbo equalizer, the target of the signal processing is $\underline{v}[k] = \underline{\rho}_{\text{dd}}[k' = k + \delta]$ ($k \in \{0, \dots, (K-1)\}$). Thus, a part of $\underline{\rho}_{\text{dd}}$ is extracted as $\underline{v}[k]$. Figure 4 visualizes the relationship between $\underline{v}[k]$, $\underline{\rho}_{\text{dd}}[b]$, and $\underline{s}_{\text{d}}[b]$. As can be seen in the figure, when $\delta + (K-1) \leq \frac{B}{2} - 1$, the second term of Eq. (40) is disappeared because the minimum value of $(i+B-b)$ is larger than $B/2$ and $\underline{s}_{\text{d}}[i+B-b > B/2]$ is always zero. Thus, $\underline{\rho}_{\text{dd}}[b]$ is rewritten as

$$\underline{\rho}_{\text{dd}}[b] = \frac{1}{\sqrt{B}} \sum_{i=0}^{(B-1)-b} \underline{\xi}[i+b] \underline{s}_{\text{d}}[i+b] \underline{\xi}^*[i] \underline{s}_{\text{d}}^*[i]. \quad (41)$$

Taking into account that $\underline{s}_{\text{d}}[b] = 0$ at $i < \theta$ or $i > \theta + (K-1)$ due to the spectrum shaping of \mathbf{M}_θ , $\underline{v}[k]$ is classified into

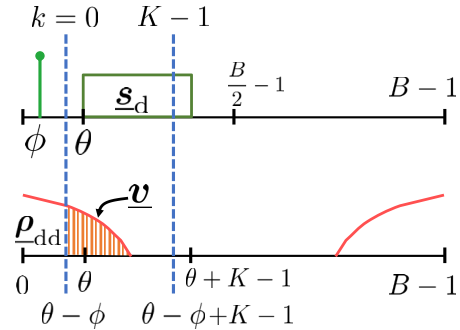


Fig. 4 Relationship between $\underline{v}[k]$, $\rho_{\text{dd}}[b]$, and $\underline{s}_{\text{d}}[b]$.

two cases:

if $k > (K-1) - \delta$,

$$\underline{v}[k] = 0. \quad (42)$$

Otherwise, denoting $k' = k + \delta$,

$$\begin{aligned} \underline{v}[k] &= \frac{1}{\sqrt{B}} \sum_{i=\theta}^{(K-1)+\theta-k'} \underline{\xi}[i+k'] \underline{s}_{\text{d}}[i+k'] \underline{\xi}^*[i] \underline{s}_{\text{d}}^*[i] \\ &= \frac{1}{\sqrt{B}} \sum_{i=\theta}^{(K-1)+\theta-k'} \underline{\xi}[i+k'] \underline{x}[i+k'-\theta] \underline{\xi}^*[i] \underline{x}^*[i-\theta] \\ &= \frac{1}{\sqrt{B}} \sum_{i=0}^{(K-1)-k'} \underline{\xi}[i+k'+\theta] \underline{x}[i+k'] \underline{\xi}^*[i+\theta] \underline{x}^*[i] \\ &= \frac{1}{\sqrt{B}} \sum_{i=0}^{(K-1)-(k+\delta)} \zeta[i, k] \underline{x}[i+k+\delta] \underline{x}^*[i], \end{aligned} \quad (43)$$

where we have

$$\zeta[i, k] = \underline{\xi}[i+k+\theta+\delta] \underline{\xi}^*[i+\theta]. \quad (44)$$

In the following discussion, only the cases of $k \leq (K-1) - \delta$ are dealt because $\underline{v}[k > (K-1) - \delta] = 0$. The conditional expectation of $\underline{v}[k]$ is given by

$$\begin{aligned} \hat{v}[k] &= \frac{1}{\sqrt{B}} \sum_{i=0}^{(K-1)-(k+\delta)} \zeta[i, k] \\ &\cdot \mathbb{E}_\lambda \{ \underline{x}[i+k+\delta] \underline{x}^*[i] \}. \end{aligned} \quad (45)$$

Here, we approximate that the correlation between $\underline{x}[i+k+\delta]$ and $\underline{x}[i]$ under the condition λ is negligibly small. (45) is rewritten as

$$\begin{aligned} \hat{v}[k] &= \frac{1}{\sqrt{B}} \sum_{i=0}^{(K-1)-(k+\delta)} \zeta[i, k] \\ &\cdot \mathbb{E}_\lambda \{ \underline{x}[i+k+\delta] \} \mathbb{E}_\lambda \{ \underline{x}^*[i] \}, \end{aligned} \quad (46)$$

Thanks to the simple linear algebra, the vector form of $\mathbb{E}_\lambda \{ \underline{x}[k] \}$ is given by

$$\mathbb{E}_\lambda \{ \underline{\mathbf{x}} \} = \mathbf{F}_K \mathbb{E}_\lambda \{ \mathbf{x} \}. \quad (47)$$

When 2^Q QAM is utilized for signaling, $x[k]$ is determined

by Q coded bits: $\mathbf{c}[k] = [c[Qk], \dots, c[Q(k+1) - 1]]^T$. The other coded bits are independent of the symbol $x[k]$. Therefore, the constituent element of the conditional expectation $\mathbb{E}_\lambda\{\mathbf{x}\}$ in (47) is defined by

$$\begin{aligned} \hat{x}[k] &= \mathbb{E}_\lambda\{x[k]\} = \sum_{x \in \mathcal{X}} x \Pr[x[k] = x | \lambda] \\ &= \sum_{x \in \mathcal{X}} x \Pr[\mathbf{c}[k] = \mathbf{Q}[x] | \lambda[k]] \\ &= \sum_{x \in \mathcal{X}} x \prod_{l=0}^{Q-1} \Pr[c[Qk+l] = \tilde{c}_l | \lambda[Qk+l]], \end{aligned} \quad (48)$$

where \mathcal{X} represents a set of constellations and $\mathbf{Q}[x] = [\tilde{c}_0, \dots, \tilde{c}_{Q-1}]^T$ denotes constituent coded bits of the symbol x . The constituent probability in Eq. (48) is derived by

$$\Pr[c[l] = 1 | \lambda[l]] = \frac{\exp(\lambda[l])}{1 + \exp(\lambda[l])}, \quad (49)$$

$$\Pr[c[l] = 0 | \lambda[l]] = \frac{1}{1 + \exp(\lambda[l])}. \quad (50)$$

3.2.2 Variance of Residual Interference in Frequency Domain $g[k]$

We need to derive the variance of the residual interference in frequency domain $g[k]$, which is formulated as

$$g[k] = \mathbb{E}_\lambda \left\{ |v[k] - \hat{v}[k]|^2 \right\} = \mathbb{E}_\lambda \left\{ |v[k]|^2 \right\} - |\hat{v}[k]|^2. \quad (51)$$

The conditional expectation of $|v[k]|^2$ is given by

$$\begin{aligned} &\mathbb{E}_\lambda \left\{ |v[k]|^2 \right\} \\ &= \sum_{i=0}^{(K-1)-(k+\delta)} \frac{|\zeta[i, k]|^2}{B} \mathbb{E}_\lambda \left\{ |\underline{x}[i+k+\delta] \underline{x}^*[i]|^2 \right\} \\ &= \sum_{i=0}^{(K-1)-(k+\delta)} \sum_{j=0}^{(K-1)-(k+\delta)} \frac{|\zeta[i, k]|^2}{B} \\ &\quad \cdot \mathbb{E}_\lambda \left\{ \underline{x}[i+k+\delta] \underline{x}^*[i] \underline{x}^*[j+k+\delta] \underline{x}[j] \right\}. \end{aligned} \quad (52)$$

Furthermore, the conditional expectation in Eq. (52) can be classified into four cases as follows:

- If $i = j$,

$$\mathbb{E}_\lambda \left\{ |\underline{x}[i+k+\delta]|^2 \right\} \mathbb{E}_\lambda \left\{ |\underline{x}[i]|^2 \right\}. \quad (53)$$

- If $i+k+\delta = j$,

$$\mathbb{E}_\lambda \{ \underline{x}^2[j] \} \mathbb{E}_\lambda \{ \underline{x}^*[i] \} \mathbb{E}_\lambda \{ \underline{x}^*[j+k+\delta] \}. \quad (54)$$

- If $j+k+\delta = i$,

$$\mathbb{E}_\lambda \{ \underline{x}[i+k+\delta] \} \mathbb{E}_\lambda \{ (\underline{x}^2[i])^* \} \mathbb{E}_\lambda \{ \underline{x}[j] \}. \quad (55)$$

- Others,

$$\mathbb{E}_\lambda \{ \underline{x}[i+k+\delta] \} \mathbb{E}_\lambda \{ \underline{x}^*[i] \} \mathbb{E}_\lambda \{ \underline{x}[j+k+\delta]^* \} \mathbb{E}_\lambda \{ \underline{x}[j] \}. \quad (56)$$

The expectations $\mathbb{E}_\lambda \{ x^2[i] \}$ and $\mathbb{E}_\lambda \{ |x[i]|^2 \}$ are given by

$$\mathbb{E}_\lambda \{ x^2[i] \} \simeq \hat{x}^2[i], \quad (57)$$

$$\begin{aligned} \mathbb{E}_\lambda \{ |x[i]|^2 \} &= \mathbb{E}_\lambda \{ \underline{x}[i] \} \circ \mathbb{E}_\lambda \{ \underline{x}[i] \}^* \\ &\quad - \sum_{k=0}^{K-1} \left(\mathbb{E}_\lambda \{ |x[k]|^2 \} - |\hat{x}[k]|^2 \right), \end{aligned} \quad (58)$$

where $\mathbb{E}_\lambda \{ |x[k]|^2 \}$ is given by

$$\mathbb{E}_\lambda \{ |x[k]|^2 \} = \sum_{x \in \mathcal{X}} |x|^2 \Pr[\mathbf{c}[k] = \mathbf{Q}[x] | \lambda[k]]. \quad (59)$$

Note that the detailed derivation of these expectations are described in Appendix B. As a result, the variance $g[k]$ is computed by Eq. (51)–Eq. (59).

3.3 Channel Estimation

3.3.1 For Signal Detection

For the signal detection, the estimation of $\underline{h} = \sqrt{K} \mathbf{F}_K \mathbf{h}$ is required. To deal with the requirement, we use Golay sequence [14] as a training sequence $\mathbf{x}_G = [x_G[0], \dots, x_G[K-1]]^T$ with symbol energy E_s , which is transmitted before data transmissions. In this case, the time domain representation of the received signal Eq. (24) is given by

$$\begin{aligned} \mathbf{y}_G &= \mathbf{F}_K^H \underline{\mathbf{y}}_G = \mathbf{F}_K^H (\underline{\mathbf{H}} \mathbf{x}_G + \underline{\mathbf{v}} + \underline{\mathbf{z}}) \\ &= \mathbf{H} \mathbf{x}_G + \mathbf{F}_K^H (\underline{\mathbf{v}} + \underline{\mathbf{z}}), \end{aligned} \quad (60)$$

where \mathbf{y}_G indicates the received signal of the training sequence \mathbf{x}_G and \mathbf{H} is a circulant matrix defined by

$$\mathbf{H} = \mathbf{F}_K^H \underline{\mathbf{H}} \mathbf{F}_K. \quad (61)$$

Denoting the channel impulse response, which has τ memory taps, by the first column vector of \mathbf{H} : $\mathbf{h} = [\mathbf{h}'^T, \mathbf{O}_{1 \times (K-\tau)}]^T \in \mathbb{C}^{K \times 1}$ and $\mathbf{h}' = [h[0], \dots, h[\tau-1]]^T$, Eq. (60) can be rewritten as

$$\mathbf{y}_G = \mathbf{X}_G \mathbf{h}' + \mathbf{F}_K^H (\underline{\mathbf{v}} + \underline{\mathbf{z}}), \quad (62)$$

where $\mathbf{X}_G \in \mathbb{C}^{K \times \tau}$ is a circulant matrix based on \mathbf{x}_G , which is represented as

$$\mathbf{X}_G = \begin{bmatrix} x_G[0] & x_G[K-1] & \cdots & x_G[K-\tau+1] \\ x_G[1] & x_G[0] & \cdots & x_G[K-\tau+2] \\ \vdots & \vdots & \cdots & \vdots \\ x_G[K-1] & x_G[K-2] & \cdots & x_G[K-\tau] \end{bmatrix}. \quad (63)$$

The length of τ is typically set at the CP length, since the number of taps of CIR is usually within the CP length.

In order to find \mathbf{h}' , the least square (LS) estimation is available. In the LS channel estimation, \mathbf{h} is determined by

$$\hat{\mathbf{h}} = \begin{bmatrix} \mathbf{X}_G^\dagger \mathbf{y}_G \\ \mathbf{O}_{(K-\tau) \times 1} \end{bmatrix} = \begin{bmatrix} \frac{1}{KE_s} \mathbf{X}_G^H \mathbf{y}_G \\ \mathbf{O}_{(K-\tau) \times 1} \end{bmatrix}, \quad (64)$$

where \mathbf{X}_G^\dagger represents the pseudo-inverse matrix of \mathbf{X}_G , which is given by $\mathbf{X}^H/(KE_s)$, thanks to the significant sharpness of the autocorrelation of the Golay sequence. When the length of the Golay sequence is sufficiently long, the harmful impacts of noise and interference can be mitigated. As a result, \underline{h} is estimated by $\hat{\underline{h}} = \sqrt{K}F_K\hat{h}$.

3.3.2 For Generation of Soft Interference Replica

For the generation of soft interference replica, $\zeta[i, k] = \underline{\xi}[i + k + \theta + \delta]\underline{\xi}^*[i + \theta]$ is necessary. According to Eq. (26), relationship between $\underline{h}[i]$ and $\underline{\xi}[\theta + i]$ is expressed as $\underline{h}[i] = \sqrt{\frac{B}{E_p}}\underline{\xi}^*[\phi]\underline{\xi}[\theta + i]$, then $\zeta[i, k]$ is reproduced by

$$\underline{\xi}[\theta + i] = \frac{\sqrt{B}\underline{h}[i]}{\sqrt{E_p}\underline{\xi}^*[\phi]}, \quad (65)$$

$$\zeta[i, k] = \frac{B}{E_p|\underline{\xi}[\phi]|^2}\underline{h}[i + k + \delta]\underline{h}^*[i]. \quad (66)$$

To estimate $\zeta[i, k]$, we can use the \hat{h} of Eq. (64). In addition, $E_p|\underline{\xi}[\phi]|^2$ is also necessary to estimate. Assuming weak frequency selectivity of the channel, $|\underline{\xi}[\phi]|$ is closed to $|\underline{\xi}[\theta]|$ when we assign a sufficiently small value to δ . Therefore, $|\underline{\xi}[\phi]|^2$ is given by

$$\begin{aligned} \underline{\xi}[\phi] &\simeq \underline{\xi}[\theta] = \frac{\sqrt{B}\underline{h}[0]}{\sqrt{E_p}\underline{\xi}^*[\phi]}, \\ |\underline{\xi}[\phi]|^2 &= \frac{\sqrt{B}\underline{h}[0]}{\sqrt{E_p}}. \end{aligned} \quad (67)$$

Eventually, $\zeta[i, k]$ is estimated by

$$\hat{\zeta}[i, k] = \frac{\sqrt{B}}{\sqrt{E_p}\hat{\underline{h}}[0]}\hat{h}[i + k + \delta]\hat{h}^*[i]. \quad (68)$$

Moreover, the variance of the noise can be also estimated in the training period. The samples of noise are given by

$$\hat{\underline{z}}_G = \underline{y}_G - \hat{\mathbf{H}}\underline{x}_G - \hat{\underline{v}}_G, \quad (69)$$

where $\hat{\underline{v}}_G$ can be generated from the training sequence. Thus, the unbiased variance is expressed as $N_0 = \frac{1}{(K-1)}\hat{\underline{z}}_G^H\hat{\underline{z}}_G$.

4. EXIT Chart Based LDPC Code Design

According to the turbo principle, the performance of iterative detection depends on the exchange of extrinsic LLRs. Thus, a visualization of the iterative behavior helps in improving the detection capability. At first, we introduce EXIT chart analysis [8] to visualize the iterative behavior of extrinsic LLRs. LLR sequence itself is inconvenient for evaluating the reliability measure. In the EXIT chart, extrinsic LLR sequence is transformed into scalar-valued mutual information

(MI) in the range of 0.0 to 1.0.

Let $\boldsymbol{\chi} = [\chi[0], \dots, \chi[L-1]]^T$ be a vector LLR of coded bits \mathbf{c} . When the LLR $\boldsymbol{\chi}$ is symmetrical distribution, the MI of $\boldsymbol{\chi}$ is found by [8], [15]

$$\mathcal{T}(\boldsymbol{\chi}) = 1 - \frac{1}{L} \sum_{l=0}^{L-1} \log_2 \left[1 + e^{-(2c[l]-1)\chi[l]} \right]. \quad (70)$$

MI's for equalizer and decoder output are given by $I_E = \mathcal{T}(\boldsymbol{\gamma})$ and $I_D = \mathcal{T}(\boldsymbol{\lambda})$, respectively. Note that I_E and I_D are identical to decoder and equalizer inputs, respectively. When $I_D \approx 1.0$ after several iterations, the perfect knowledge about the coded bits \mathbf{c} is obtained, resulting in error-free detection. Our interest is whether the error-free detection is achievable or not. EXIT functions of equalizer and decoder help to predict the achievability. The EXIT functions represent the input-output relations of MI, which are represented as

$$I_E = \mathcal{F}_E(I_D) : \text{Equalizer}, \quad (71)$$

$$I_D = \mathcal{F}_D(I_E) : \text{Decoder}. \quad (72)$$

The EXIT chart exhibits both of the two functions in one figure to visualize the achievable points of trajectory of MI exchange. The examples of the EXIT chart are shown in Fig. 5 of higher and lower $E_b/N_0 = \mathbb{E}\{\beta^H\beta/B\}/N_0$, respectively. E_β indicates received power without noise, more specifically,

$$\begin{aligned} E_\beta &= \frac{1}{B} \text{tr}[\boldsymbol{\Xi}^H \boldsymbol{\Xi}](KE_s + E_p) \\ &= (1 + R_E) \frac{K}{B} E_s \text{tr}[\boldsymbol{\Xi}^H \boldsymbol{\Xi}], \end{aligned} \quad (73)$$

where we have the pilot-to-signal power ratio (PSR): $R_E = E_p/(KE_s)$. The parameters for drawing the EXIT charts are summarized in Table 1. The parity check matrix of the LDPC code is optimized for AWGN channels ($\delta = K$), in terms of

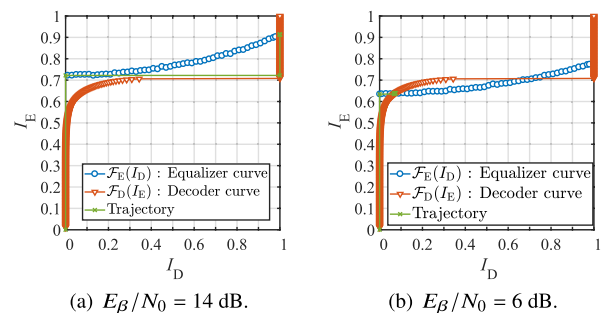


Fig. 5 Examples of EXIT chart at PSR = 6 dB.

Table 1 Parameters of EXIT chart examples.

| | |
|---|--------------|
| Code rate | 2/3 |
| Modulation | 16 QAM |
| Channel model | Back to back |
| Size of the data symbol block K | 128 |
| Number of whole frequency bins B | 1024 |
| Frequency offset of the pilot tone ϕ | 0 |
| Frequency gap between the pilot and the data δ | 1 |

BER. Two curves of EXIT functions $\mathcal{F}_E(I_D)$ and $\mathcal{F}_D(I_E)$ are drawn by measuring output MI of Eq. (70) while yielding prior LLR with the arbitrary MI which meets the consistency condition [16]. The trajectory indicates measured MI during the empirical iterative process. The two curves imply upper and lower bounds of the trajectory.

Now, let us focus on Fig. 5(a). At the first iteration, the trajectory starts from $I_D = 0$ since no feedback is provided from the decoder. Without the cancellation process, the equalizer outputs LLR with $I_E = \mathcal{F}_E(0) = 0.8$. The resultant LLR is forwarded to the decoder, then the decoder outputs LLR with $I_D = \mathcal{F}_D(0.8) = 1$. As the result, error-free decoding is achievable in this scenario. Figure 5(a) implies the fact that the trajectory can reach $I_D = 1$ if the tunnel between two EXIT curves open. On the other hand, two curves intersect before reaching $I_D = 1$ in Fig. 5(b), due to the closed tunnel. In this case, the achievable MI is $I_D = 0.05$, which is subject to detection errors.

The problem arising here is how to open the tunnel between two EXIT curves. We have three options: (i) Improve E_β/N_0 , (ii) Widen δ , (iii) Design LDPC code. The goal of this paper is to improve receiver sensitivity. Therefore, the option (i) should be out of focus. On top of that, δ should be as narrow as possible, in terms of the cost of the receiver. Therefore, irregularity of the parity check matrix of LDPC code should be appropriately designed.

In order to characterize the behavior of the equalizer, Fig. 6 plots equalizer EXIT curves in several conditions. The figure explicitly tell us that the EXIT property depends not only on E_β/N_0 but also R_E . Recalling Eq. (20), it is obvious that the energy of the pilot-signal beat components is in proportion to $E_s E_p$. Moreover, $E_s E_p \propto \frac{(E_\beta)^2 R_E}{K(1+R_E)^2}$ is maximized at $R_E = 0$ dB. The fact indicates that I_E is highest at $R_E = 0$ dB while perfectly cancelling the interference at $I_D = 1$. Note that higher I_E implies that E_β/N_0 can be reduced. However, when it is subject to residual interference due to imperfect cancelling, E_s should be smaller than E_p because the energy of the interference $|v[k]|^2$ is in proportion to $|x[i+k+\delta]x^*[i]|^2$ as shown in Eq. (43). Thus, $R_E = 0$ dB is no longer optimal in the presence of the interference. As proof, $R_E = 8$ dB achieve the highest I_E at $I_D = 0$ in Fig. 6(a).

For realizing error-free detection while utilizing LDPC optimized for AWGN of Fig. 5, initial equalizer output $\mathcal{F}_E(0)$

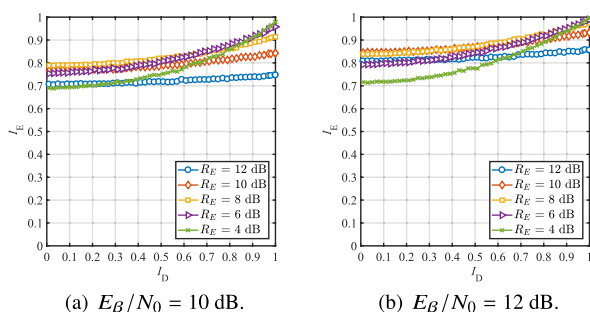


Fig. 6 EXIT functions of equalizer.

should be higher than 0.8. Note that the practical decoder EXIT property deviates from the theoretical curve, thus here we set upward margin of 0.1 for the error-free detection. As shown in Fig. 6(b), the cases of $R_E = 8$ –12 dB obviously satisfy the requirement of $\mathcal{F}_E(0) > 0.8$. Therefore, the LDPC is suitable for archiving the error-free detection in the range of $E_\beta/N_0 > 12$ dB.

Now, let our focus shift to lower E_β/N_0 of Fig. 6(a). There is no case to satisfy the requirement of $\mathcal{F}_E(0) > 0.8$. The inconvenience motivates us to design an appropriate irregular LDPC code, which opens the tunnel between two EXIT curves [8], [17]. The EXIT curves of the designed LDPC are depicted in Fig. 7. The characteristics of the LDPC is mostly depending on a degree-distribution of the parity check matrix. The degree-distribution indicates the arrangement of 1 in the parity check matrix. We have optimized the degree-distributions which is showed in Table 2. The column's degree denoted in Table 2 means that the number of ones included in a column, and row's degree is that of a row. Thus, Table 2 summarizes the ratio of those degrees in the entire parity check matrix.

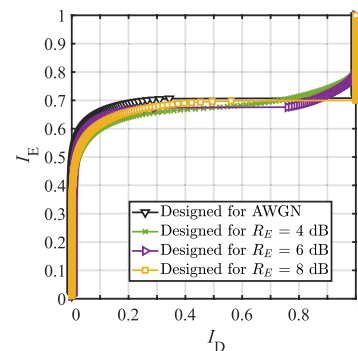


Fig. 7 EXIT chart of designed LDPCs.

Table 2 Parameters of degree distribution.

| PSR = 4 dB | | | | |
|-----------------|------|------|------|------|
| Column's degree | 2 | 3 | 8 | |
| Ratio | 0.75 | 0.06 | 0.19 | |
| Row's degree | 9 | 10 | 11 | |
| Ratio | 0.25 | 0.47 | 0.28 | |
| PSR = 6 dB | | | | |
| Column's degree | 2 | 8 | | |
| Ratio | 0.72 | 0.28 | | |
| Row's degree | 11 | 12 | | |
| Ratio | 0.67 | 0.33 | | |
| PSR = 8 dB | | | | |
| Column's degree | 2 | 3 | 4 | |
| Ratio | 0.42 | 0.4 | 0.18 | |
| Row's degree | 9 | 10 | 11 | |
| Ratio | 0.04 | 0.8 | 0.16 | |
| For AWGN | | | | |
| Column's degree | 2 | 3 | 4 | 8 |
| Ratio | 0.34 | 0.24 | 0.21 | 0.21 |
| Row's degree | 11 | 12 | 13 | |
| Ratio | 0.04 | 0.8 | 0.16 | |

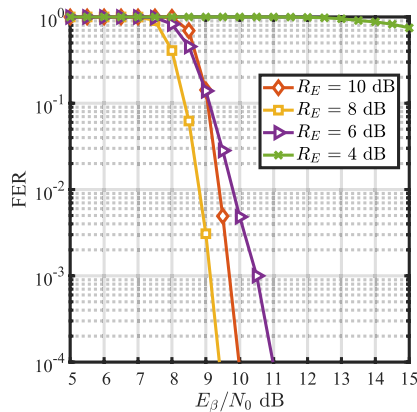
5. Performance Evaluations by Computer Simulation

Computer simulations were conducted to verify the performances of the proposed iterative soft IC and its LDPC design. Table 3 summarizes the parameters of the computer simulations. Decoding algorithm of the LDPC is SPA and the number of internal iterations is 50.

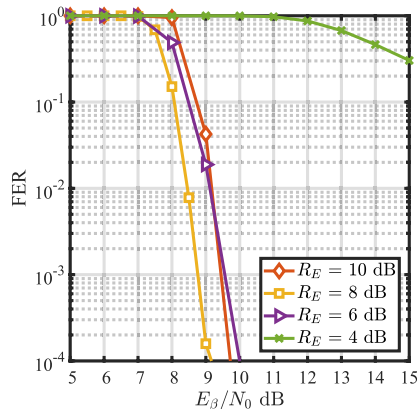
Figure 8 shows frame error rate (FER) performances of LDPC optimized for AWGN, where Fig. 8(a) is the case without IC (the number of iterations = 1) and Fig. 8(b) is the case with iterative soft IC (the number of iterations = 6). At first, Fig. 8(a) indicates that the importance of PSR adjust-

Table 3 Simulation parameters.

| | |
|---|--------------|
| Code word length | 2000 |
| Code rate | 2/3 |
| Decoding algorithm | SPA |
| Internal iteration number of LDPC | 50 |
| Modulation | 16 QAM |
| Channel model | Back to back |
| Size of the data symbol block K | 128 |
| Number of whole frequency bins B | 1024 |
| Frequency gap between the pilot and the data δ | 1 |
| Number of iterations for cancellation | 1 or 6 |



(a) Number of iteration 1.

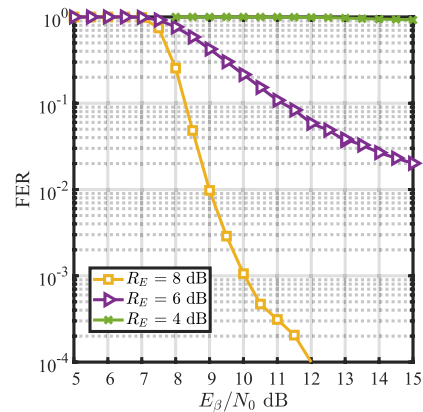


(b) Number of iteration 6.

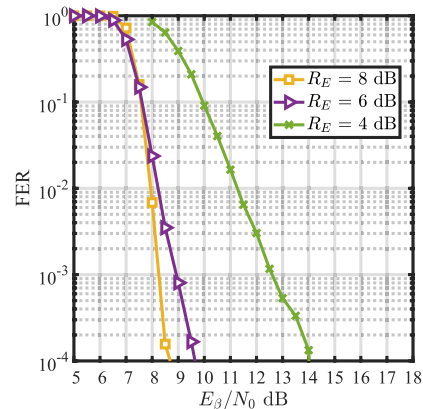
Fig. 8 FER performances where LDPC optimized for AWGN.

ment. For example, PSR $R_E = 8$ dB achieves $FER = 10^{-3}$ at the lowest E_{β}/N_0 . As shown in Fig. 6(a) in the case of $R_E \geq 10$ dB, although the impact of the interference is less than that of $R_E = 8$ dB, the noise tolerance is deteriorated. Therefore, $R_E = 8$ dB is the best performance in the case without IC. Moreover, Fig. 8(a) shows that the iterative soft IC brings very small improvement if the LDPC is optimized for AWGN. As shown in Fig. 5, when using the LDPC optimized for AWGN, the output MI of the decoder $I_D = \mathcal{F}_D(I_E)$ steeply reaches 1. Therefore, when the tunnel between two curves opens, the error-free detection can be achieved even in the first iteration.

Figure 9 characterizes FER of LDPC optimized for each R_E . Comparing Fig. 9(a) and Fig. 9(b), the effect of the soft IC is explicitly depicted. In Fig. 9(b), the case of $R_E = 8$ dB is the best performance, and achieves $FER = 10^{-3}$ at $E_{\beta}/N_0 = 8.2$ dB. It is about 0.5 dB lower than the case of Fig. 8(b). This result implies the fact that the proposed IC with the LDPC optimized for the equalizer curve of $R_E = 8$ dB is capable of improving the performance of signal detection. On the other hand, the performances of $R_E = 4, 6$ dB are superior to the cases of Fig. 8(b) at same R_E , they cannot overcome the best performance. Recalling Fig 6(a), the shapes of the curve of $R_E = 4, 6$ dB seem to be suitable for



(a) Without IC.



(b) With iterative soft IC.

Fig. 9 FER performances where LDPC optimized for the equalizer curve.

the equalizer curves. However, the right end ($I_D = 1$) of the curves is not higher than that of $R_E = 8$ dB, which indicates that the performance of $R_E = 4, 6$ dB cannot overcome that of $R_E = 8$ dB even if the soft IC works effectively. Furthermore, at the low E_B/N_0 , the left side ($I_D = 0$) of the curve is too low, resulting in an intersect with decoder's curve. Thus, the case of $R_E = 8$ dB is the optimal regardless of the IC.

To be honest, the interference is negligibly small for 16 QAM at the optimal PSR, and the iterative gain of the proposed design seems to be slight. However, we are confident that the negative impact of such interference becomes significant while utilizing high-order QAM. In such a case, the proposed turbo equalizer is expected to be more efficient.

6. Conclusions

This paper proposed an iterative soft IC referred to as turbo equalizer for the self-coherent detection, and EXIT chart based irregular LDPC code optimization for the turbo equalizer in optical fiber short-reach transmissions. The self-coherent detection captures pilot-signal beat components as the desired signals, while suppressing interference caused by signal-signal beat components. To improving the performance of the self-coherent detection, the turbo equalizer with the aid of FEC decoder was proposed. Furthermore, we explicitly clarified the fact that the typical FEC code is not appropriate for turbo equalizers. Therefore, we designed an appropriate LDPC code in terms of EXIT analysis. The validity of the proposed turbo equalizer with optimized LDPC is confirmed by the computer simulations. This technique will open new vistas for minimizing the distance between pilot tone and data spectrum, which means lower bandwidth for DSP without sacrificing throughput, in the self-coherent systems.

Acknowledgements

This work was financially supported by JSPS KAKENHI Grant Number JP18H03231, Japan.

References

- [1] S.J. Savory, "Digital coherent optical receivers: Algorithms and subsystems," *IEEE J. Sel. Topics Quantum Electron.*, vol.16, no.5, pp.1164–1179, Sept. 2010.
- [2] A.J. Lowery and J. Armstrong, "Orthogonal-frequency-division multiplexing for dispersion compensation of long-haul optical systems," *Opt. Express*, vol.14, no.6, pp.2079–2084, March 2006.
- [3] M. Schuster, S. Randel, C.A. Bunge, S.C.J. Lee, F. Breyer, B. Spinnler, and K. Petermann, "Spectrally efficient compatible single-sideband modulation for OFDM transmission with direct detection," *IEEE Photon. Technol. Lett.*, vol.20, no.9, pp.670–672, May 2008.
- [4] W.R. Peng, B. Zhang, K.M. Feng, X. Wu, A.E. Willner, and S. Chi, "Spectrally efficient direct-detected OFDM transmission incorporating a tunable frequency gap and an iterative detection techniques," *J. Lightwave Technol.*, vol.27, no.24, pp.5723–5735, Dec. 2009.
- [5] A. Mecozzi, C. Antonelli, and M. Shtaif, "Kramers–Kronig coherent receiver," *Optica*, vol.3, no.11, pp.1220–1227, Nov. 2016.
- [6] L. Hanzo, T. Liew, and B. Yeap, *Turbo Coding, Turbo Equalisation and Space-Time Coding*, Wiley, 2002.
- [7] T. Matsumoto, S. Ibi, S. Sampei, and R.S. Thomä, "Adaptive transmission with single-carrier multilevel BICM," *Proc. IEEE*, vol.95, no.12, pp.2354–2367, Dec. 2007.
- [8] S.T. Brink, G. Kramer, and A. Ashikhmin, "Design of low-density parity-check codes for modulation and detection," *IEEE Trans. Commun.*, vol.52, no.4, pp.670–678, April 2004.
- [9] H.G. Myung, J. Lim, and D.J. Goodman, "Single carrier FDMA for uplink wireless transmission," *IEEE Veh. Technol. Mag.*, vol.1, no.3, pp.30–38, Sept. 2006.
- [10] L. Martoyo, T. Weiss, F. Capar, and F.K. Jondral, "Low complexity CDMA downlink receiver based on frequency domain equalization," *2003 IEEE 58th Veh. Technol. Conf.*, vol.2, pp.987–991, Oct. 2003.
- [11] V.A. Bogatyrev, M.M. Bubnov, E.M. Dianov, A.S. Kurkov, P.V. Mamyshev, A.M. Prokhorov, S.D. Rummyantsev, V.A. Semenov, S.L. Semenov, A.A. Sysoliatin, S.V. Chernikov, A.N. Gur'yanov, G.G. Devyatikh, and S.I. Miroshnichenko, "A Single-Mode Fiber With Chromatic Dispersion Varying Along the Length," *J. Lightwave Technol.*, vol.9, no.5, pp.561–566, May 1991.
- [12] S. Ibi, T. Matsumoto, R.S. Thomä, S. Sampei, and N. Morinaga, "EXIT chart-aided adaptive coding for multilevel BICM with turbo equalization in frequency-selective MIMO channels," *IEEE Trans. Veh. Technol.*, vol.56, no.6, pp.3757–3769, Nov. 2007.
- [13] S. Haykin, *Adaptive Filter Theory*, 4th ed., Prentice Hall, Upper Saddle River, NJ, 2002.
- [14] M.J.E. Gelay, "Multi-slit spectrometry," *J. Opt. Soc. Am.*, vol.39, no.6, pp.437–444, June 1949.
- [15] M. El-Hajjar and L. Hanzo, "EXIT charts for system design and analysis," *IEEE Commun. Surveys Tuts.*, vol.16, no.1, pp.127–153, 2014.
- [16] M. Tüchler, S.T. Brink, and J. Hagenauer, "Measures for tracing convergence of iterative decoding algorithms," *Proc. 4th IEEE/ITG Conf. on Source and Channel Coding*, pp.53–60, 2002.
- [17] G. Lechner, J. Sayir, and I. Land, "Optimization of LDPC codes for receiver frontends," *2006 IEEE Int. Symp. on Inf. Theory*, pp.2388–2392, July 2006.

Appendix A: Detailed Derivations of Beat Components

The signal-pilot beat ρ_{dp} is expanded as

$$\begin{aligned} \rho_{dp} &= \left(\mathbf{F}_B^H \Xi \mathbf{F}_B \mathbf{s}_d \right) \circ \left(\mathbf{s}_p^H \mathbf{F}_B^H \Xi^H \mathbf{F}_B \right)^T \\ &= \left(\frac{1}{\sqrt{B}} [\mathbf{f}_{B,0}, \dots, \mathbf{f}_{B,B-1}]^H \Xi \mathbf{F}_B \mathbf{s}_d \right) \\ &\quad \circ \left(\frac{1}{\sqrt{B}} \mathbf{s}_p^H \mathbf{F}_B^H \Xi^H [\mathbf{f}_{B,0}, \dots, \mathbf{f}_{B,B-1}] \right)^T \\ &= \frac{1}{B} \begin{bmatrix} \mathbf{f}_{B,0}^H \Xi \mathbf{F}_B \mathbf{s}_d \\ \vdots \\ \mathbf{f}_{B,B-1}^H \Xi \mathbf{F}_B \mathbf{s}_d \end{bmatrix} \circ \begin{bmatrix} \mathbf{s}_p^H \mathbf{F}_B^H \Xi^H \mathbf{f}_{B,0} \\ \vdots \\ \mathbf{s}_p^H \mathbf{F}_B^H \Xi^H \mathbf{f}_{B,B-1} \end{bmatrix}. \quad (\text{A.1}) \end{aligned}$$

The elements of ρ_{dp} are expressed as

$$\rho_{dp}[b] = \frac{1}{B} \mathbf{f}_{B,b}^H \Xi \mathbf{F}_B \mathbf{s}_d \left(\mathbf{F}_B \mathbf{s}_p \right)^H \Xi^H \mathbf{f}_{B,b}. \quad (\text{A.2})$$

From (7), denoting $\mathbf{i}_\phi = [\mathbf{O}_{1 \times \phi}, 1, \mathbf{O}_{1 \times (B-\phi-1)}]^T$, we have

$$\left(\mathbf{F}_B \mathbf{s}_p \right)^H = \sqrt{E_p} \mathbf{i}_\phi^T. \quad (\text{A.3})$$

Substituting it into (A.2), $\rho_{dp}[k]$ is expressed as

$$\begin{aligned}
\rho_{\text{dp}}[b] &= \frac{1}{B} \mathbf{f}_{B,b}^H \underline{\Xi} \mathbf{F}_B \mathbf{s}_d \sqrt{E_p} \mathbf{i}_\phi^T \underline{\Xi}^H \mathbf{f}_{B,b} \\
&= \frac{1}{B} \mathbf{f}_{B,b}^H \underline{\Xi} \mathbf{F}_B \mathbf{s}_d \sqrt{E_p} e^{-j2\pi \frac{b\phi}{B}} \underline{\xi}^*[\phi] \\
&= \frac{1}{B} e^{-j2\pi \frac{b\phi}{B}} \sqrt{E_p} \underline{\xi}^*[\phi] \mathbf{f}_{B,b}^H \underline{\Xi} \mathbf{F}_B \mathbf{s}_d. \quad (\text{A}\cdot 4)
\end{aligned}$$

Denoting a phase rotation matrix $\Theta_\phi = \text{diag}[\mathbf{f}_{B,\phi}]$, the vector form of $\rho_{\text{dp}}[b]$ is given by

$$\begin{aligned}
\rho_{\text{dp}} &= \sqrt{\frac{E_p}{B}} \underline{\xi}^*[\phi] \Theta_\phi \mathbf{F}_B^H \underline{\Xi} \mathbf{F}_B \mathbf{s}_d \\
&= \sqrt{\frac{E_p}{B}} \underline{\xi}^*[\phi] \Theta_\phi \underline{\Xi} \mathbf{s}_d. \quad (\text{A}\cdot 5)
\end{aligned}$$

Secondly, the pilot-pilot beat $\rho_{\text{pp}}[b]$ is expanded as

$$\begin{aligned}
\rho_{\text{pp}}[b] &= \frac{1}{B} \mathbf{f}_{B,b}^H \underline{\Xi} (\mathbf{F}_B \mathbf{s}_p) (\mathbf{F}_B \mathbf{s}_p)^H \underline{\Xi}^H \mathbf{f}_{B,b} \\
&= \frac{1}{B} \mathbf{f}_{B,b}^H \underline{\Xi} (\sqrt{E_p} \mathbf{i}_\phi) (\sqrt{E_p} \mathbf{i}_\phi)^T \underline{\Xi}^H \mathbf{f}_{B,b} \\
&= \frac{E_p}{B} |\underline{\xi}[\phi]|^2. \quad (\text{A}\cdot 6)
\end{aligned}$$

Thus, the vector form of $\rho_{\text{pp}}[b]$ is simply given by

$$\rho_{\text{pp}} = \frac{E_p}{B} |\underline{\xi}[\phi]|^2 \mathbf{1}_{B \times 1}. \quad (\text{A}\cdot 7)$$

Finally, the signal-signal beat $\rho_{\text{dd}}[b]$ is expanded as

$$\begin{aligned}
\rho_{\text{dd}}[b] &= \frac{1}{B} \mathbf{f}_{B,b}^H \underline{\Xi} (\mathbf{F}_B \mathbf{s}_d) (\mathbf{F}_B \mathbf{s}_d)^H \underline{\Xi}^H \mathbf{f}_{B,b} \\
&= \frac{1}{B} \mathbf{f}_{B,b}^H \underline{\Xi} \mathbf{s}_d \mathbf{s}_d^H \underline{\Xi}^H \mathbf{f}_{B,b} \\
&= \frac{1}{B} \left[\sum_{i=0}^{B-1} \underline{\xi}[i] \underline{s}_d[i] e^{j2\pi \frac{i b}{B}} \right] \cdot \left[\sum_{j=0}^{B-1} \underline{\xi}[j] \underline{s}_d[j] e^{j2\pi \frac{j b}{B}} \right]^* \\
&= \frac{1}{B} \sum_{i=0}^{B-1} \sum_{j=0}^{B-1} \left\{ e^{j2\pi \frac{(i-j)b}{B}} \underline{\xi}[i] \underline{s}_d[i] \underline{\xi}^*[j] \underline{s}_d^*[j] \right\}. \quad (\text{A}\cdot 8)
\end{aligned}$$

Appendix B: Detailed Derivations of the Variance of Interference

At first, $\mathbb{E}_\lambda \{x^2[i]\}$ is the i -th element of $\mathbb{E}_\lambda \{\underline{\mathbf{x}} \circ \underline{\mathbf{x}}\}$ which is given by

$$\begin{aligned}
\mathbb{E}_\lambda \{\underline{\mathbf{x}} \circ \underline{\mathbf{x}}\} &= \mathbb{E}_\lambda \{\underline{\mathbf{x}}\} \circ \mathbb{E}_\lambda \{\underline{\mathbf{x}}\} \\
&= \begin{bmatrix} \sum_{k=0}^{K-1} (\mathbb{E}_\lambda \{x^2[k]\} - |\mathbb{E}_\lambda \{x[k]\}|^2) e^{-j2\pi \frac{2k \cdot 0}{K}} \\ \vdots \\ \sum_{k=0}^{K-1} (\mathbb{E}_\lambda \{x^2[k]\} - |\mathbb{E}_\lambda \{x[k]\}|^2) e^{-j2\pi \frac{2k \cdot i}{K}} \\ \vdots \\ \sum_{k=0}^{K-1} (\mathbb{E}_\lambda \{x^2[k]\} - |\mathbb{E}_\lambda \{x[k]\}|^2) e^{-j2\pi \frac{2k \cdot (K-1)}{K}} \end{bmatrix} \\
&+ \frac{1}{K} \begin{bmatrix} \sum_{k=0}^{K-1} (\mathbb{E}_\lambda \{x^2[k]\} - |\mathbb{E}_\lambda \{x[k]\}|^2) e^{-j2\pi \frac{2k \cdot 0}{K}} \\ \vdots \\ \sum_{k=0}^{K-1} (\mathbb{E}_\lambda \{x^2[k]\} - |\mathbb{E}_\lambda \{x[k]\}|^2) e^{-j2\pi \frac{2k \cdot i}{K}} \\ \vdots \\ \sum_{k=0}^{K-1} (\mathbb{E}_\lambda \{x^2[k]\} - |\mathbb{E}_\lambda \{x[k]\}|^2) e^{-j2\pi \frac{2k \cdot (K-1)}{K}} \end{bmatrix}
\end{aligned}$$

$$\begin{aligned}
&= \mathbb{E}_\lambda \{\underline{\mathbf{x}}\} \circ \mathbb{E}_\lambda \{\underline{\mathbf{x}}\} \\
&+ (\mathbf{F}_K \circ \mathbf{F}_K) (\mathbb{E}_\lambda \{\mathbf{x} \circ \mathbf{x}\} - \mathbb{E}_\lambda \{\mathbf{x}\} \circ \mathbb{E}_\lambda \{\mathbf{x}\}). \quad (\text{A}\cdot 9)
\end{aligned}$$

Although $(\mathbf{F}_K \circ \mathbf{F}_K) (\mathbb{E}_\lambda \{\mathbf{x} \circ \mathbf{x}\} - \mathbb{E}_\lambda \{\mathbf{x}\} \circ \mathbb{E}_\lambda \{\mathbf{x}\})$ is difficult to compute by simple fast Fourier transform, $\mathbb{E}_\lambda \{x^2[i]\}$ is not dominant in $\underline{v}[k]$, moreover, $\sum_{k=0}^{K-1} (\mathbb{E}_\lambda \{x^2[k]\} - |\mathbb{E}_\lambda \{x[k]\}|^2) e^{-j2\pi \frac{2k \cdot i}{K}}$ becomes a tiny value compared to $\mathbb{E}_\lambda \{\underline{\mathbf{x}}\} \circ \mathbb{E}_\lambda \{\underline{\mathbf{x}}\}$. Therefore, the term shall be ignored, resulting in $\mathbb{E}_\lambda \{x^2[i]\} = \mathbb{E}_\lambda \{x[i]\}^2$.

On the other hand, $\mathbb{E}_\lambda \{\underline{\mathbf{x}} \circ \underline{\mathbf{x}}^*\}$ is computed by

$$\begin{aligned}
\mathbb{E}_\lambda \{\underline{\mathbf{x}} \circ \underline{\mathbf{x}}^*\} &= \mathbb{E}_\lambda \{\underline{\mathbf{x}}\} \circ \mathbb{E}_\lambda \{\underline{\mathbf{x}}\}^* \\
&= \begin{bmatrix} \sum_{k=0}^{K-1} (\mathbb{E}_\lambda \{|x[k]\}^2) - |\mathbb{E}_\lambda \{x[k]\}|^2 \\ \vdots \\ \sum_{k=0}^{K-1} (\mathbb{E}_\lambda \{|x[k]\}^2) - |\mathbb{E}_\lambda \{x[k]\}|^2 \\ \vdots \\ \sum_{k=0}^{K-1} (\mathbb{E}_\lambda \{|x[k]\}^2) - |\mathbb{E}_\lambda \{x[k]\}|^2 \end{bmatrix} \\
&+ \frac{1}{K} \begin{bmatrix} \sum_{k=0}^{K-1} (\mathbb{E}_\lambda \{|x[k]\}^2) - |\mathbb{E}_\lambda \{x[k]\}|^2 \\ \vdots \\ \sum_{k=0}^{K-1} (\mathbb{E}_\lambda \{|x[k]\}^2) - |\mathbb{E}_\lambda \{x[k]\}|^2 \\ \vdots \\ \sum_{k=0}^{K-1} (\mathbb{E}_\lambda \{|x[k]\}^2) - |\mathbb{E}_\lambda \{x[k]\}|^2 \end{bmatrix} \\
&= \mathbb{E}_\lambda \{\underline{\mathbf{x}}\} \circ \mathbb{E}_\lambda \{\underline{\mathbf{x}}\}^* \\
&- \sum_{k=0}^{K-1} (\mathbb{E}_\lambda \{|x[k]\}^2) - |\mathbb{E}_\lambda \{x[k]\}|^2 \mathbf{1}_{K \times 1}. \quad (\text{A}\cdot 10)
\end{aligned}$$

Eventually, we have

$$\begin{aligned}
\mathbb{E}_\lambda \{x^2[i]\} &= \mathbb{E}_\lambda \{x[i]\} \circ \mathbb{E}_\lambda \{x[i]\}^* \\
&- \sum_{k=0}^{K-1} (\mathbb{E}_\lambda \{|x[k]\}^2) - |\mathbb{E}_\lambda \{x[k]\}|^2. \quad (\text{A}\cdot 11)
\end{aligned}$$



Noboru Osawa received the B.E. and M.E. degrees in communication engineering from Osaka University, Osaka, Japan, in 2014 and 2016. He is currently pursuing the Ph.D. degree at the Graduate School of Engineering, Osaka University. His research interests include digital signal processing in wireless and optical communication field, interference cancellation, and iterative detection. He is a member of IEEE.



Shinsuke Ibi received the B.E. degree in advanced engineering from Suzuka College of Technology, Japan, in 2002, and the M.E. and Ph.D. degrees in communication engineering from Osaka University, Japan, in 2004 and 2006, respectively. From 2005 to 2006, he was a visiting researcher at the Centre for Wireless Communications, University of Oulu, Finland. In 2006, he joined the Graduate School of Engineering, Osaka University, and he is currently an Associate Professor in the Department of Information and Communications Technology, Osaka University.

From 2010 to 2011, he was a visiting researcher at the University of Southampton, UK. His research interests include EXIT-based coding theory, iterative detection, stochastic digital signal processing, and communication theory. He received the 64th and 71st Best Paper Awards from IEICE, and the 24th Telecom System Technology Award from the Telecommunication Advancement Foundation. He is a member of IEEE.



Koji Igarashi received the B.E. degree in electrical and computer engineering from Yokohama National University, Yokohama, Japan, in 1997, and the M.E. and Ph.D. degrees in electronic engineering from the University of Tokyo, Tokyo, Japan, in 1999 and 2002, respectively. From 2002 to 2004, he was with the Furukawa Electric Corporation, Ltd. Since 2004, he was with the University of Tokyo. From 2007 to 2011, he was an Assistant Professor, earlier at the Department of Frontier Informatics, and then,

the Department of Electrical Engineering and Information Systems. From 2012 to 2013, he was with KDDI R&D Laboratories, Inc., and currently an Associate Professor at the Department of Electrical, Electronic and Information Engineering, Osaka University, Osaka, Japan. He is also a Visiting Researcher at KDDI R&D Laboratories, Inc. His current research interests include high-capacity long-haul optical fiber transmission systems, signal processing for coherent optical communication systems, and optical devices for space-division multiplexed optical transmission systems.



Seiichi Sampei received the B.E., M.E., and Ph.D. degrees in electrical engineering from Tokyo Institute of Technology, Japan, in 1980, 1982, and 1991, respectively. From 1982 to 1993, he was with the Communications Research Laboratory, Ministry of Posts and Telecommunications. From 1991 to 1992, he was a visiting researcher at the University of California, Davis. In 1993, he joined the Faculty of Engineering, Osaka University, and he is currently a Professor in the Department of Information and Communications Technology, Osaka University.

He has been involved in the development of adaptive modulation, intelligent radio transmission/access, cognitive wireless networking, and wireless distributed network techniques. He received the Shinohara Young Engineering Award, the Achievements Award, the Communications Society Best Paper Award, the Best Paper Award from IEICE, the Telecom System Technology Award from the Telecommunication Advancement Foundation, the DoCoMo Mobile Science Award from the Mobile Communication Fund, the Ericsson Telecommunications Award, and Shida Rinzaburo Award from the President of Council for Info-Communications Promotion Month. He is a member of the Institute of Image Information and Television Engineers (ITE) and a Fellow of IEEE.